Mechatronic Design and Positioning Accuracy Characterisation of a Robotic Arm for Exploration Rovers

Retrieval of the dielectric properties of a resonant material in the terahertz region via self-detection near field optical microscopy

Carlo Silvestri, Lorenzo Luigi Columbo, Massimo Brambilla

***Abstract*—We present a numerical and analytical study of the self-detection scattering type near field optical microscopy (SD s-SNOM), a recently demonstrated technique based on a combination of self-mixing interferometry and scattering near-field microscopy. This scheme, which exploits a terahertz (THz) quantum cascade laser as both a laser source and detector, allows to investigate the optical properties of resonant materials in the THz range with resolution far beyond the diffraction limit. Our study, developed by using a modified version of the Lang-Kobayashi model, is focused on the weak feedback regime (Acket parameter $C \approx 10^{-1}$), where we derive an approximated method for the retrieval of the scattering coefficient of the SD s-SNOM configuration applied to a sample of Cesium Bromide (CsBr). These results were used in turn to derive the dielectric permittivity of the sample, reporting a good accuracy in the estimation of its phonon resonances.**

***Index Terms*—SNOM, Dielectric function, Atomic Force Microscope, Quantum Cascade Laser, Self-Mixing**

I. Introduction

ELECTROMAGNETIC waves with frequency in the Terahertz (THz) spectral range provide a tool for characterization and analysis of materials and biological systems presenting their resonances in this spectral region. Scattering-type scanning near-field optical microscopy (s-SNOM) is a technique which allows to investigate the optical properties of a material sample with subwavelength spatial resolution, by circumventing the diffraction limit [1], [2]. In s-SNOM, the light beam is conveyed onto an atomic force microscope (AFM) nanometric tip placed in proximity of the material sample surface. The near-field interaction between probe and sample mediated by evanescent waves modifies amplitude and phase of the light scattered by the probe and subsequently detected by far-field methods detectors, allowing the retrieval of the optical properties of the sample with nanoscale resolution, limited only by the dimension of the tip apex radius (typically 10-100 nm) [3]–[8]. In SNOM setups, the tip typically operates in tapping mode, oscillating at frequencies around 100 KHz, so that the detected scattered signal can be demodulated at an integer multiple of the tip vibration frequency through a lock-in amplifier, and the pure information about the near-field interaction can be retrieved by extracting the background-free harmonics (typically the third harmonic is considered).

However, the lack of efficient detectors is one of the main issues in the THz range. Recently, a new setup has been demonstrated based on the combination of s-SNOM with a self-mixing interferometry scheme, where the laser itself is used as a detector [9]. In this configuration, named self-detection (SD) s-SNOM, the exploited light source is a THz quantum cascade laser (QCL), and the measured signal is the voltage across the laser terminals. The SD s-SNOM has been exploited to analyze phonon resonant materials and topological insulators in the very weak feedback (VWF), and weak feedback (WF) regime with the QCL operating in single mode [9]–[11], and frequency comb operation [12]. **Therefore, the advancement provided by the SD s-SNOM for the performance of a phase-resolved THz nano-imaging is two-fold, combining the advantages of both self-mixing interferometry and s-SNOM. In fact, on the one hand it makes up for the scarcity of efficient detectors in the THz range, on the other it provides high resolution far beyond the diffraction limit. Moreover, the self-alignment of the experimental layout constitutes a further point of advantage of this technique.**

In this work we study from the analytical and numerical point of view the SD s-SNOM configuration in the WF regime. **The commonly exploited approaches for the study of this technique available in the literature deal with the VWF regime, where an unpertubed emission frequency of the laser can be assumed, condition which simplifies the mathematical description [9]. Here, we overcome this assumption, by taking into account first order corrections to the VWF theory, providing then analytical approximated formulas valid in the WF regime. The passage from VWF to WF is relevant because it allows to investigate regimes where the power of the detected signal is higher, assuring an improvement for the retrieval of the sample's dielectric properties, and providing potentially better definition in imaging.** We develop an approach to retrieve information about the sample by describing the single-mode dynamics of a THz QCL subject to optical feedback through the Lang-Kobayashi (LK) equations [13]. **We specialize the LK equations to this particular scheme** by introducing a complex scattering coefficient σ, which models the interaction between AF tip and analyzed sample, and embodies the dielectric properties of the material sample. **The proposed method is particularly significant for two main reasons: firstly, it relies on convenient analytical reconstruction**

C. Silvestri, is with the School of Information Technology and Electrical Engineering, The University of Queensland, Brisbane, QLD 4072, Australia.

L.L. Columbo is with the Dipartimento di Elettronica e Telecomunicazioni, Politecnico di Torino, 10129 Torino, Italy.

M. Brambilla is with the Dipartimento Interateneo di Fisica, Politecnico di Bari and CNR-IFN, UOS Bari, Italy.

formulas whose application requires a limited number of experimental measurements; secondly, in the WF regime we show that this method reduces the errors in retrieval with respect to commonly used approaches, only rigorously valid in the VWF [10]. The material sample is supposed to be Cesium Bromide (CsBr), which exhibits a Reststrahlen band in the THz region, delimited by a transverse optical (TO) phonon resonance at 73 cm^{-1}, and a longitudinal optical (LO) phonon resonance at 110 cm^{-1}. **It will be shown that the proposed approach provides high accuracy in the estimation for such resonances.**

In Sec. II we present a description and schematic of the SD s-SNOM experimental layout. In Sec. III we introduce the theoretical model, and we provide an approximated treatment of the steady state solutions of the LK equations by using first-order truncated Taylor expansions of the laser frequency around the free running emission frequency, in place of relying on the commonly used zero-order model. In Sec. IV we provide a first order approximated method for the retrieval of the scattering coefficient from a set of simulated self-mixing signals, and we numerically test this method, verifying that it provides more accurate results in the WF regime with respect to the zero-order approach. Sec. V is dedicated to the reconstruction of harmonics of the scattering coefficient from the harmonics of self-mixing signals, and we show also in this case that an improvement in the accuracy is achieved if the first order is taken into account in presence of WF. In Sec. VI we reconstruct the dielectric permittivity of the CsBr by using the previously introduced first order methods for the scattering coefficient retrieval, identifying with good accuracy the position of the phonon resonances. Finally, Sec. VII draws the conclusions of the work.

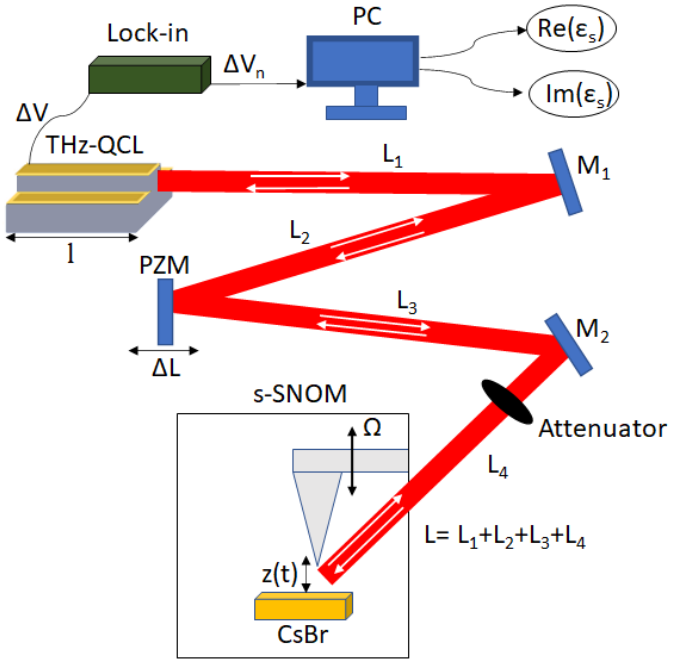

Fig. 1. **Experimental layout for the SD s-SNOM technique. The light emitted by a THz QCL is conveyed onto the target, which consists of an AFM tip operating in tapping mode, placed in proximity of the material sample, in this case CsBr. Then, the light is backscattered by the target and partially reinjected into the laser cavity. An attenuator is placed in the configuration, in order to control the optical feedback intensity. The oscillation frequency of the tip is Ω, and the distance between the tip apex and the surface of the sample is the time-dependent quantity $z(t)$, expressed by Eq. (6) in Sec. III. The total distance between the laser and the AFM tip is L. M_1 and M_2 are fixed mirrors, while PZM is a piezoelectric mirror which can be displaced to generate a variation ΔL of the external cavity length L. We indicate with l the length of the QCL cavity. The voltage signal ΔV is demodulated in harmonics ΔV_n by using a lock-in amplifier. Then, ΔV_n are used in turn to retrieve the real and imaginary part of the dielectric function of the sample ε_s.**

II. SD s-SNOM CONFIGURATION

For sake of clarity in this section we resume the SD s-SNOM configuration and working principle as described for example in [9]. A scheme of the SD s-SNOM layout is shown in Fig. 1. The laser source is a single-mode THz QCL, which is also exploited as a detector, according to the self-mixing scheme. The QCL cavity has length l. The THz beam emitted by the QCL travels a path determined by two fixed mirrors M_1 and M_2, and a piezoelectric mirror PZM. The beam, having propagated a total distance L, is finally focused onto an AFM tip placed in proximity of the CsBr material sample. The near-field interaction between tip and sample generates a scattered field which is re-injected into the laser cavity by the same optical components. An optical attenuator allows to vary the intensity of the re-injected beam, selecting the operating feedback regime. The re-injected field modifies the emission characteristics of the QCL, such as emission frequency, output power, and voltage across the laser terminals ΔV, which is the detected self-mixing signal. By measuring ΔV, in fact, it is possible to retrieve the target properties, and to map the optical response with nanometric resolution. The AFM tip operates in tapping mode, i.e. oscillates with frequency Ω, so that the distance between the tip apex and the sample surface is a time-dependent function $z(t)$. This allows to demodulate the voltage signal ΔV in harmonics of the tapping frequency by means of a lock-in amplifier, and the measured harmonic amplitudes ΔV_n are recorded. In this way, by considering the harmonics above a certain order (typically $n \geq 3$), it is possible to exclude the spurious background contribution and isolate the near-field interaction that nonlinearly depends on the tip-target distance. We remark that the movable piezo-actuated mirror PZM appearing in the setup, consents to vary the light path length by a determined quantity ΔL. It will be shown in Sections IV and V how this aspect is fundamental for the retrieval of the information about the optical properties of the sample.

III. THEORETICAL MODEL

A. Lang-Kobayashi equations with complex scattering coefficient

The single mode THz dynamics is described by a modified form of the LK equations, where we introduced the complex scattering σ, which models the interaction between AF tip

and and analyzed sample [9], [10]. The LK equations for the electric field E and the density of carriers N in the SD s-SNOM read:

$$\frac{dE(t)}{dt} = \frac{1}{\tau_p}\left[\frac{1}{2}(1+i\alpha)\left(N-1\right)E + \tau_p \kappa E(t-\tau)e^{-i\omega_0\tau}\right] \quad (1)$$

$$\frac{dN(t)}{dt} = \frac{1}{\tau_e}\left[I_p - N\left(1-|E|^2\right)\right] \quad (2)$$

$$\kappa = \sigma\frac{a(1-R)}{\tau_c\sqrt{R}} \quad (3)$$

where κ is the complex coupling coefficient, τ_e is the carrier lifetime, τ_p is the photon lifetime, α is the linewidth enhancement factor, $\tau = \frac{2L}{c}$ is the roundtrip time in the external cavity of the configuration, L is the length of the external cavity **(distance between the laser and the AFM tip apex)**, ω_0 is the angular frequency of the propagating wave, I_p is the pump parameter, R is the reflectivity equal for both the QCL facets, τ_c is the roundtrip time in the laser cavity, a is a factor related to an optical attenuator present in the experimental setup. The coefficient $\sigma = Se^{i\phi}$, whose modulus and phase are respectively S and ϕ, is the ratio between the field scattered by the target and the incident field onto the target, and obviously includes the dielectric properties of the sample probed by the oscillating tip. For this reason, a retrieval of σ is crucial in order to reconstruct the dielectric function of the investigated material [3], [9], [10].

The parameter C, is the Acket parameter which defines the level of feedback of the considered configuration, is:

$$C = \frac{aS\tau(1-R)}{\tau_c\sqrt{R}}\sqrt{1+\alpha^2} \quad (4)$$

Since C depends on the scattering coefficient modulus S, in principle, a retrieval of S allows to quantify the feedback parameter.

In our treatment the interaction between tip and sample is modeled by using the finite dipole (FD) model [3], where the tip **in presence of an incident field** is assumed to be a spheroid which polarizes the sample, which in turn interacts with the tip. In the FD model an effective polarizability α_{eff} of the tip when it lies at distance z from the sample surface is introduced, which depends on the geometric parameters of the configurations and on the dielectric permittivity of both the tip and the sample, respectively ε_t, and ε_s (for further details, see the Supplementary materials). In particular, α_{eff} depends on ε_s through the response function β, expressed by:

$$\beta = \frac{\varepsilon_s - 1}{\varepsilon_s + 1} \quad (5)$$

We model the tip movement assuming that the tip apex-sample distance varies sinusoidally:

$$z(t) = z_A + z_A\cos(2\pi\Omega t) \quad (6)$$

where z_A is the amplitude and Ω the frequency of the oscillations. The collected feedback signal will be thus oscillating and demodulated via a lock-in amplifier, retrieving its harmonics. Since the tip oscillation occurs with a frequency of 10-100 KHz, we can safely analyze our model using the steady state solutions of Eqs. (1)–(2), since typical time rates for a QCL are in the 10-100 GHz range.

B. Steady-state solutions

The steady-state solutions of Eqs. (1)–(2) are retrieved by imposing the conditions $E(t)$=$E_s exp(-i\omega_F t)$, $N(t)$=N_s, and introducing $\Delta V = 1 - N_s$, which is a quantity proportional to the terminal voltage of the QCL [14], obtaining:

$$\Delta V = VS\cos\left(\omega_F\tau - \phi\right) \quad (7)$$

$$\omega_F\tau = \omega_0\tau - \varepsilon S\sqrt{1+\alpha^2}\sin\left(\omega_F\tau - \phi + \arctan\left(\alpha\right)\right) \quad (8)$$

where ω_F is the angular frequency of the laser in presence of feedback, and the quantities V and ε are expressed by:

$$V = 2\frac{1-R}{\sqrt{R}}a\frac{\tau_p}{\tau_c} \quad (9)$$

$$\varepsilon = \frac{\tau}{\tau_c}\left(\frac{1-R}{\sqrt{R}}\right)a \quad (10)$$

Eqs. (7)-(8) show how the optical properties of the sample shape the measured signal. We highlight that ε is linked to the feedback parameter C by $\varepsilon = \frac{C}{S\sqrt{1+\alpha^2}}$.

C. The weak regime: approximated expressions for the steady state solutions

In vast literature the so called VWF regime is considered by assuming $\omega_F\tau \approx \omega_0\tau$ (that corresponds to $C << 1$) [14], [15]. This approximation is not valid in case of higher feedback, a condition which allows better signal to noise ratio (SNR) and appreciation of higher order harmonics in the signal retrieval. We propose an approach valid for WF regimes ($C \approx 10^{-1}$) based on an expansion of the phase excess equation (8). We can reasonably assume ε small, and we are allowed to use Taylor series expansions. By keeping the first order terms, we retrieve the approximated expression for ω_F and ΔV:

$$\omega_F\tau = \omega_0\tau - \varepsilon S\sqrt{1+\alpha^2}\sin(\Phi_0 + \widetilde{\beta}) \quad (11)$$

$$\Delta V = VS\{\cos\Phi_0 + \varepsilon S'\sin\Phi_0\sin\Phi_0'\} \quad (12)$$

where:

$$\Phi_0 = \omega_0\tau - \phi, \quad (13)$$

$$\Phi_0' = \omega_0\tau - \phi + \arctan(\alpha), \quad (14)$$

$$S' = S\sqrt{1+\alpha^2} \quad (15)$$

$$\widetilde{\beta} = \arctan(\alpha). \quad (16)$$

In the next section we show how to retrieve S and ϕ exploiting Eqs. (11)-(12).

IV. Reconstruction of the scattering coefficient

A. Zero-order reconstruction

The VWF case corresponds to retain only terms of zero-order in ϵ in Eqs. (11)-(12):

$$\Delta V \approx VS\cos\left(\Phi_0\right) \quad (17)$$

$$\omega_F \approx \omega_0 \quad (18)$$

assuming thus a frequency unperturbed by the optical feedback. We now introduce a phase variation of $\pi/2$ in Φ_0, assuming that a new measurement is performed **by considering a value $L+\Delta L$ of the laser-tip distance, with $\Delta L = \frac{\lambda_0}{8}$, that can be introduced in the experimental setup by displacing the piezoelectric mirror PZM (see Fig. 1). We specify that λ_0 is the reference emission wavelength expressed by $\lambda_0 = \frac{2\pi c}{\omega_0}$. When this is substituted in the definition of τ and subsequently in Eq. (7), the self mixing signal takes the form**:

$$\Delta V_{\frac{\pi}{2}} = VS\cos\left(\Phi_0 + \frac{\pi}{2}\right) = -VS\sin\left(\Phi\right) \tag{19}$$

By combining Eqs. (17)–(19) with the same procedure followed in [9], and under the assumption that $\omega_0\tau$ is negligibly perturbed by the laser-tip distance oscillation **(we approximate $L + z(t)$ with L because $z_{\rm A} << L$)**, it is possible to retrieve explicit approximated formulas for the S and ϕ:

$$S = \frac{1}{V}\sqrt{\Delta V^2 + \Delta V_{\frac{\pi}{2}}{}^2} \tag{20}$$

$$\phi = \omega_0\tau + \arctan\left[\frac{\Delta V_{\frac{\pi}{2}}}{\Delta V}\right] \tag{21}$$

Eqs. (20)–(21) allow to determine the complex scattering coefficient through two signal measurements for two different values of distance between QCL and target.

B. First order reconstruction

Let us consider Eq. (12) again. If we halt this expansion at first order in ε, assuming a higher level of feedback in the so called WF regime ($C \approx 10^{-1}$), and consider three different values of shift of the quantity Φ_0, i.e. $\frac{\pi}{2}$, π and $\frac{3\pi}{2}$, corresponding to performing measures **with laser-tip distance given by $L + \lambda_0/8$, $L + \lambda_0/4$, and $L + 3\lambda_0/8$ respectively, where $\lambda_0 = \frac{2\pi c}{\omega_0}$ also in this case,** and introduce them into Eq. (12), we obtain:

$$\Delta V_{\frac{\pi}{2}} = VS\{-\sin\Phi_0 + \varepsilon S\sqrt{1+\alpha^2}\cos\Phi_0\cos(\Phi_0')\} \tag{22}$$

$$\Delta V_{\pi} = VS\{-\cos\Phi_0 + \varepsilon S\sqrt{1+\alpha^2}\sin\Phi_0\sin(\Phi_0')\} \tag{23}$$

$$\Delta V_{\frac{3\pi}{2}} = VS\{\sin\Phi_0 + \varepsilon S\sqrt{1+\alpha^2}\cos\Phi_0\cos(\Phi_0')\} \tag{24}$$

By using Eq. (12) and Eqs. (22)-(24), we can calculate the following differences:

$$\Delta V - \Delta V_{\pi} = 2VS\cos(\omega_0\tau - \phi) \tag{25}$$

$$\Delta V_{\frac{3\pi}{2}} - \Delta V_{\frac{\pi}{2}} = 2VS\sin(\omega_0\tau - \phi) \tag{26}$$

At this point, it is possible to determine explicit first order approximated expression for the modulus S, and the phase ϕ of the scattering coefficient:

$$S = \frac{1}{2V}\sqrt{\left(\Delta V - \Delta V_{\pi}\right)^2 + \left(\Delta V_{\frac{3\pi}{2}} - \Delta V_{\frac{\pi}{2}}\right)^2} \tag{27}$$

$$\phi = \omega_0\tau - \arctan\left(\frac{\Delta V_{\frac{3\pi}{2}} - \Delta V_{\frac{\pi}{2}}}{\Delta V - \Delta V_{\pi}}\right) \tag{28}$$

Equations (27) and (28) thus allow to reconstruct the scattering coefficient for a SD s-SNOM configuration in the WF regime, using four signals (as opposed to the zero-order reconstruction which only requires two) measured for four different values of the laser-tip distance.

C. Numerical results

We applied the predictions of Eqs. (27)–(28) in the WF regime, to derive the scattering coefficient, simulating a sample of Cesium Bromide (CsBr), a solid-state material with phonon resonances in the THz range, specifically at 73 $\rm cm^{-1}$and 110 $\rm cm^{-1}$ [16]. We choose as a value of the tip oscillation frequency $\Omega = 15380$Hz [9]. Furthermore, the tip material is Gold (Au) and its oscillation amplitude is $z_{\rm A} = 105$ nm. The full description of the sample model and adopted parameters in the framework of the FD approach is provided in the Supplementary materials, while the THz-QCL parameters we assume in our numerical study are presented in Table I. All parameters except when stated otherwise are fixed for all the simulation results presented in this work.

TABLE I
THz-QCL PARAMETERS [9].

L(m)	$\tau_{\rm p}$(ps)	$\tau_{\rm c}$(ps)	$I_{\rm p}$	α
0.6	32.4	37.4	1.5	1.5

We summarize the procedure of our numerical study in following steps:

- We choose a set of emission wavenumbers ν for the QCL between $\nu_{\rm min} = 50$ $\rm cm^{-1}$ and $\nu_{\rm max} = 140$ $\rm cm^{-1}$ with step $\Delta\nu = 0.3$ $\rm cm^{-1}$;
- For each value of ν we consider a fixed number of tip oscillation periods and solve Eqs. (7)–(8) by using the algorithm presented in [17], obtaining a time-dependent signal $\Delta V(t)$; then, we convert this signal into a function of the wavenumber by centering the time trace obtained at fixed wavenumber ν to the corresponding value ν, by using a linear conversion formula (an example of simulated self-mixing signal is shown in Fig. 2a));
- We shift the external cavity length L of $\lambda_0/8$, $\lambda_0/4$, and $3\lambda_0/8$, and we repeat the previous steps, obtaining the shifted signal $\Delta V_{\frac{\pi}{2}}$, ΔV_{π}, and $\Delta V_{\frac{3\pi}{2}}$.
- We reconstruct modulus S and phase ϕ of the scattering coefficient by using the zero-order formulas, Eqs. (20)–(21), and the first order ones, Eqs. (27)–(28).

The feedback level given by C (see the initial statements about the role of C in the LK equations) in our model is provided by Eq. (4). Since $S(t)$ is an oscillating quantity, so will be C, as Fig. 2a) shows. The feedback regime is thus designated in our work through the maximum value of C; in our parameter set we can estimate $C_{\rm max} = 0.13$. The FD model (see the Supplementary materials) provides a reference for S and ϕ, shown in Figs. 2c)-2d). The reconstructed quantities via Eqs. (27)–(28) will be compared to the corresponding plot of the same quantities calculated according to the FD model. Since the latter are independent from the feedback regime they can be

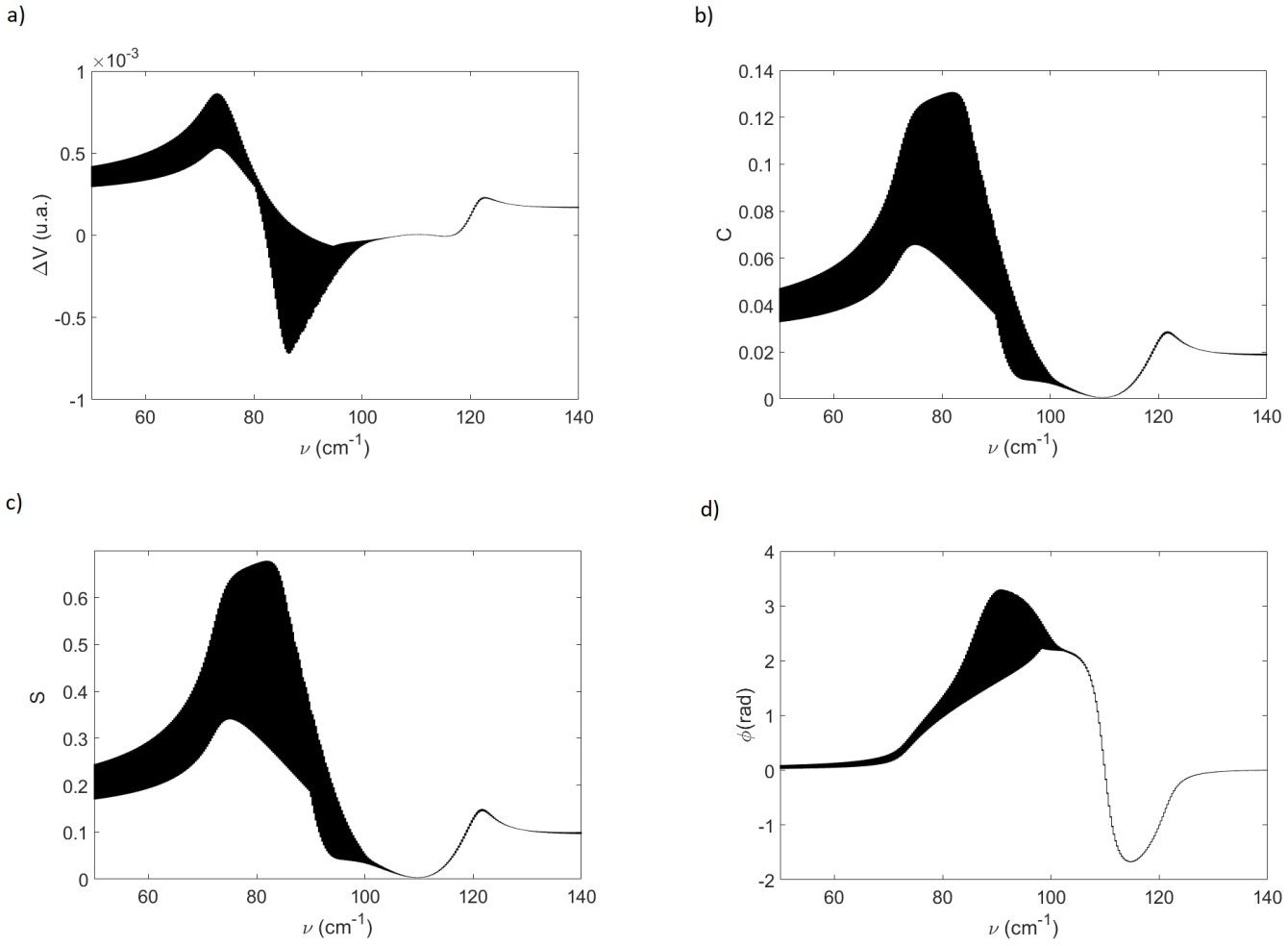

Fig. 2. a) Self-mixing signal as a function of the emission wavenumber ν for a simulation of a SD s-SNOM setup applied to a material sample of CsBr, obtained by using the parameters as in Table I, and $C_{\max} = 0.13$ (WF regime); b) corresponding plot of C as a function of the wavenumber; modulus S (c), and phase ϕ (d) of the scattering coefficient, plotted versus the wavenumber ν, calculated by using the FD model.

used as reference to evaluate the accuracy of a reconstruction of S and ϕ. In order to implement this comparison, and have a quantitative estimation of such accuracy, we introduce the indicators I_S and I_ϕ, defined as follows:

$$I_{\rm S}(\nu) = \frac{|S_{\rm calc}(\nu) - S_{\rm rec}(\nu)|}{S_{\rm calc}(\nu)} \quad (29)$$

$$I_\phi(\nu) = |\phi_{\rm calc}(\nu) - \phi_{\rm rec}(\nu)| \quad (30)$$

where $S_{\rm calc}$, $\phi_{\rm calc}$ are the quantities calculated with the FD model, and $S_{\rm rec}$, $\phi_{\rm rec}$ are the modulus and phase of the scattering coefficient reconstructed via the self-mixing signal. We remark that $I_{\rm S}$ is a relative error, while I_ϕ is an absolute one (in radians) [18].

In fig. 3 a reconstruction of S and ϕ obtained using the first order method (Eqs. (27)-(28)) is shown for $C_{\max} = 0.13$, We notice that the the reconstructed traces show a good agreement with the FD calculated plots of Figs. 2c)-d). In Fig. 4 we present the plot of the indicators (Eqs. (29)–(30)) for the first order reconstruction (red curve), and for the 0-order reconstruction (black curve), obtained by applying Eqs. (20)–(21) to the simulated self-mixing signals. Since at fixed wavenumber the calculated and reconstructed traces are oscillating quantities due to the movement of the tip, we choose as a value of the indicators $I_{\rm S}(\nu)$, $I_\phi(\nu)$ their maximum value for each value of ν. We can notice that the the first order reconstruction of S results more accurate for each value of wavenumber, with a relevant improvement in respect with the 0-order retrieval in the region between the two phonon resonances of CsBr, and around 120 $\rm cm^{-1}$. In particular the relative error $I_{\rm S}$ is always below 1% for the first order reconstruction, while it reaches the 7% in the 0-order case. A significant improvement for the phase estimation is also reached with the first order reconstruction, as shown in Fig. 4 for the indicator I_ϕ.

These results show that, as expected, when the system operates in the WF regime, accounting for the first order provides an increase in the accuracy of the reconstruction of the scattering coefficient. Since for $C_{\max} = 0.13$ we have $\varepsilon = 0.1$, an increase of the feedback level would correspond to values of $\varepsilon > 10^{-1}$, making questionable the validity of the expansions

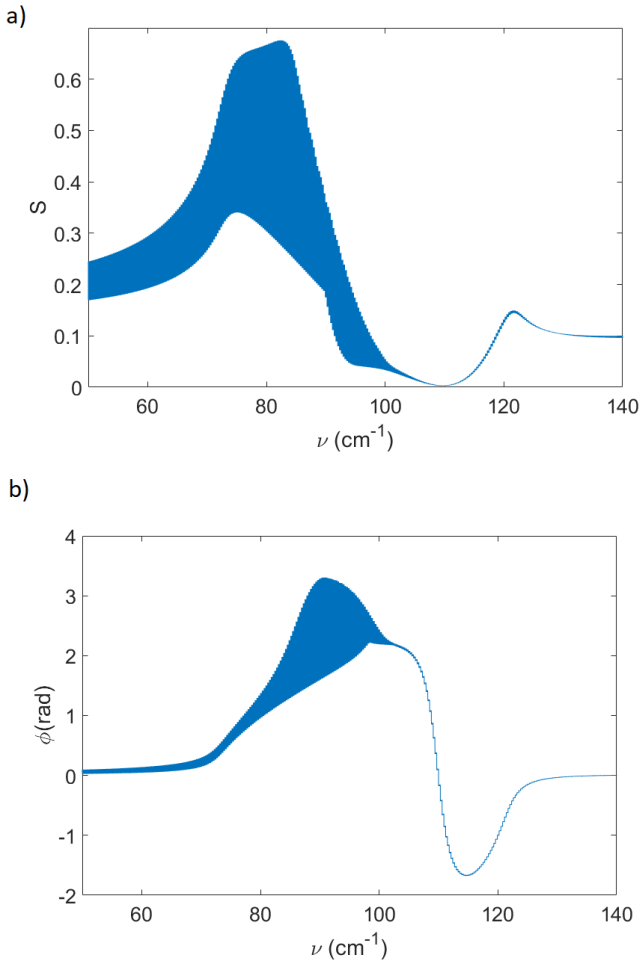

Fig. 3. Modulus S (a), and phase ϕ (b) of the scattering coefficient, plotted versus the wavenumber ν, for a SD s-SNOM configuration applied to a material sample of CsBr, reconstructed by using the first order formulas, Eqs. (27)–(28), in the case $C_{\max} = 0.13$ (operation in WF regime).

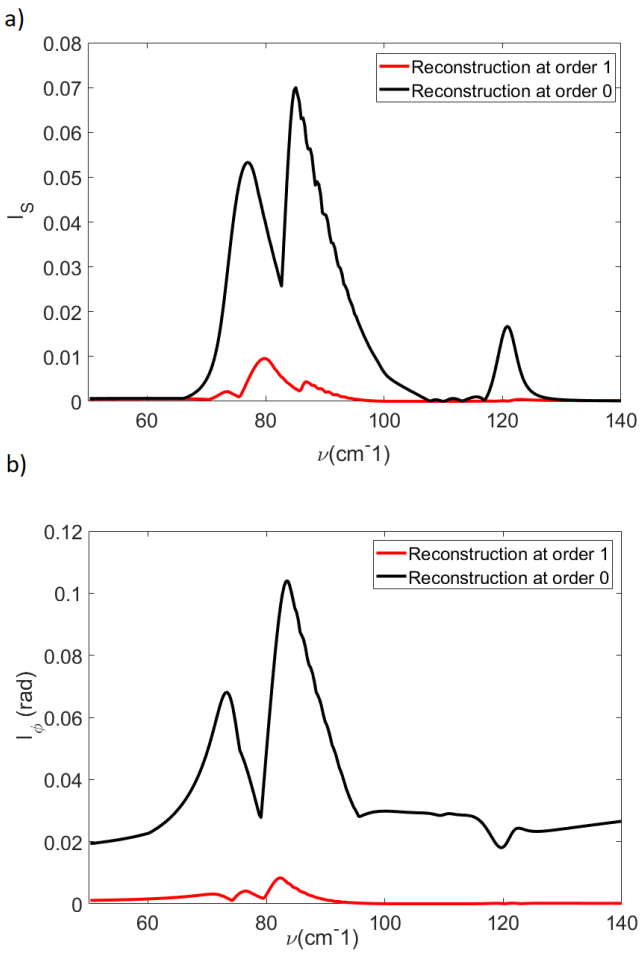

Fig. 4. Indicators $I_{\rm S}$ (a) and I_ϕ (b) as a function of the wavenumber, for the first order reconstruction obtained by using Eqs. (27)–(28) (red curve), and the zero-order reconstruction performed by using Eqs. (20)–(21) (black curve), in the case $C_{\max} = 0.13$.

on which our theory relies. We also note that as expected for values of $C_{\max} < 10^{-1}$ in the VWF regime, the accuracy advantage of the first order reconstruction becomes modest with respect to the use of the zero-order one.

V. Reconstruction of the Scattering Coefficient Harmonics

It is a commonplace that, in the experiments, the signal is analyzed by a lock-in amplifier and the harmonics are recorded [1] and exploited to retrieve the contribution of the tip-sample interaction, so that the optical properties of the sample can be extracted with consolidated methods [5], [19]. Here we consider the harmonics of our simulated feedback signal and reconstruct the harmonics of the scattering coefficient σ in the WF regime. **As shown in the following, our method provides in this regime an improved reconstruction accuracy with respect to the zero order one [9]. Moreover, we remark that as the power of the harmonics decreases with the order, the higher signal power characterizing the WF regime allows to appreciate higher order harmonics and thus a more precise estimation of σ.**

As previously mentioned, σ is an oscillating quantity due to its dependence on the effective polarizability $\alpha_{\rm eff}$, which in turn depends on the tip-sample distance through Eq. (6). It is then possible to express $\sigma(t)$ in form of the Fourier series:

$$\sigma(t) = \sum_{n=-\infty}^{\infty} \sigma_n e^{in\Omega t} = \sum_{n=-\infty}^{\infty} s_n e^{i\phi_n} e^{in\Omega t} \tag{31}$$

where $\sigma_{\rm n}$ is the generic complex Fourier coefficient of σ with modulus s_n and phase ϕ_n.

The interferometric signal ΔV as given by Eq. (7) is thus also time dependent, so that we can expand it in Fourier series:

$$\Delta V(t) = \sum_{n=-\infty}^{\infty} \Delta V_n e^{in\Omega t} \tag{32}$$

where $\Delta V_{\rm n}$ are the harmonics of the signal. In [9] it has been shown that it is possible to reconstruct $s_{\rm n}$ and $\phi_{\rm n}$ by using a

zero-order approximation with the formulas:

$$s_n = \frac{1}{V}\sqrt{(\Delta V_n)^2 + (\Delta V_{\frac{\pi}{2}})_n{}^2} \quad (33)$$

$$\phi_n = \omega_0\tau + \arctan\left[\frac{(\Delta V_{\frac{\pi}{2}})_n}{\Delta V_n}\right] \quad (34)$$

where $\Delta V_{\frac{\pi}{2}}$ are the harmonics of the self mixing signal after introducing a variation of the laser-tip distance of $\lambda_0/8$. These formulas are retrieved by assuming the approximated equalities (17)-(18) valid in the VWF regime.
In the WF regime, instead, we perform a first order reconstruction of s_n and ϕ_n, based on the following formulas (see the supplementary materials for the detailed derivation):

$$s_n = \frac{1}{2V}\sqrt{((\Delta V_{\frac{3\pi}{2}})_n - (\Delta V_{\frac{\pi}{2}})_n)^2 + (\Delta V_n - (\Delta V_\pi)_n)^2} \quad (35)$$

$$\phi_n = \omega_0\tau - \arctan\left[\frac{(\Delta V_{\frac{3\pi}{2}})_n - (\Delta V_{\frac{\pi}{2}})_n}{\Delta V_n - (\Delta V_\pi)_n}\right] \quad (36)$$

where ΔV_π, $\Delta V_{\frac{3\pi}{2}}$ are the harmonics of the signals obtained for displacements of the laser-tip distance of $\lambda_0/4$, and $3\lambda_0/8$, respectively. We can notice that the Eqs. (35)-(36) have the same mathematical structure of Eqs. (27)–(28). Therefore in the first order approximation the relation linking s_n and ϕ_n with the harmonics of four signals is the same relation linking S and ϕ with the four considered signals.

A. Numerical results

We applied Eqs. (35)-(36) for the retrieval of the scattering coefficient harmonics in the WF regime for the same parameters and sample as in the previous section. In Fig. 5 the first and zero-order reconstruction of the third harmonics of the scattering coefficient (red and black curves respectively) are presented and compared with the third harmonics of the scattering coefficient calculated with the FD model and shown in Fig. 2c)-d). The C parameter as a function of the wavenumber is shown by Fig. 2b). The trend of the reference curves is well reproduced by using both the reconstruction formulas. **However, if we look at the two insets related to the frequency region between** $70\ \mathrm{cm}^{-1}$ **and** $75\ \mathrm{cm}^{-1}$**, displayed in both the panels a) and b) of Fig. 5, we notice that the first order curves (red) better approximate the reference curves (blue) in this frequency interval.** In order to quantify precisely the accuracy **of the reconstructions**, we calculate the indicators I_{s_3} and I_{ϕ_3}, defined analogously to the previously introduced quantifiers I_S and I_ϕ (see Eqs. (29)–(30)). The plots of I_{s_3} and I_{ϕ_3} are presented in Fig. 6. We notice that the first order reconstruction of s_3 (red line) is more accurate in the entire considered wavenumber interval, with two exceptions around $80\ \mathrm{cm}^{-1}$ and $120\ \mathrm{cm}^{-1}$. These points correspond to the intersections of the FD curve (blue line in Fig. 5a)) and the zero-order reconstructed curve (black line). Conversely, the first order curve (red line) has no intersections with the reference curve, but approximates its trend better, resulting almost superimposed with it. This justifies the results in Fig. 6a).

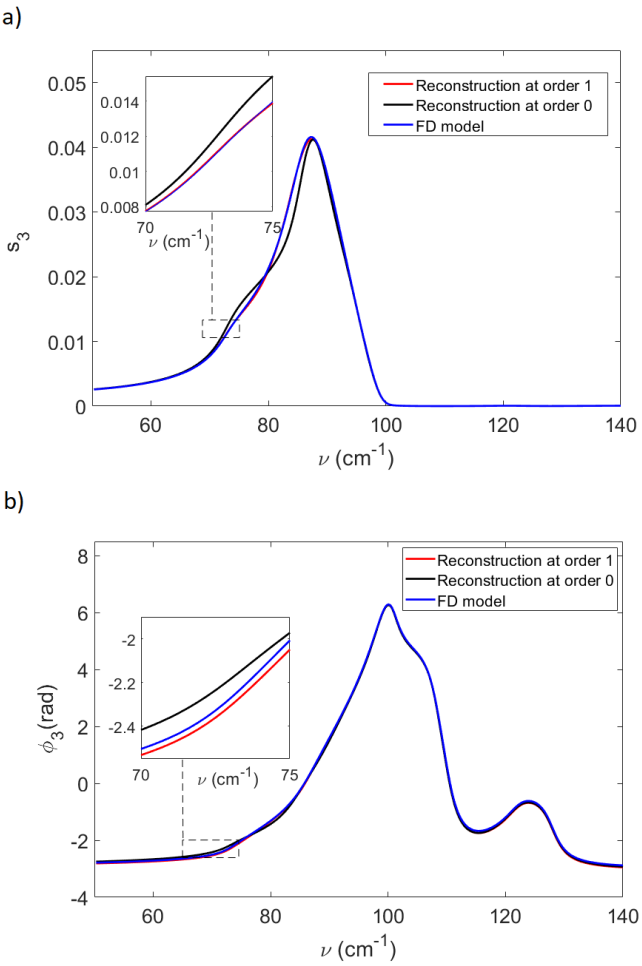

Fig. 5. Modulus s_3 (a) and phase ϕ_3 (b) of the third harmonic of the scattering coefficient as a function of the wavenumber, for the first order reconstruction obtained by using Eqs. (35)–(36) (red curve), for the zero-order reconstruction performed by using Eqs. (33)–(34) (black curve), and calculated by using the FD model (blue curve), for $C_{\max} = 0.13$. **A zoom in the frequency interval between** $70\ \mathrm{cm}^{-1}$ **and** $75\ \mathrm{cm}^{-1}$ **is displayed in two insets in both Figs. a) and b).**

In Fig. 6b) we can observe that the first order reconstruction of ϕ_3 results generally more accurate than the zero-order one, as expected, except for $\nu > 110\ \mathrm{cm}^{-1}$. In order to justify this, we firstly observe that in the same wavenumber range the reconstruction for s_3 does not exhibit this anomalous behaviour (see Fig. 6a)), suggesting that the reason is intrinsic of the reconstruction of ϕ_3. Furthermore, we notice that in the reconstruction formula for ϕ_n, Eq. (36), a fraction appears, while this is not the case for s_n. Therefore, we look at behaviour of the denominator $\Delta V_3 - (\Delta V_\pi)_3$ of Eq. (36), plotted in Fig. 7, and we notice that in the anomalous region the values of this quantity are close to zero, and the denominator oscillates between negative values and positive values crossing the horizontal axis (see the zoom in Fig. 7b)), affecting thus the efficacy of the reconstruction formula. Furthermore, if we still consider Fig. 7b), we notice that the amplitude of the oscillations are smaller in the interval $\nu > 110\ \mathrm{cm}^{-1}$ than in the remaining portion of the considered wavenumber range, and they are therefore affected by higher relative numerical

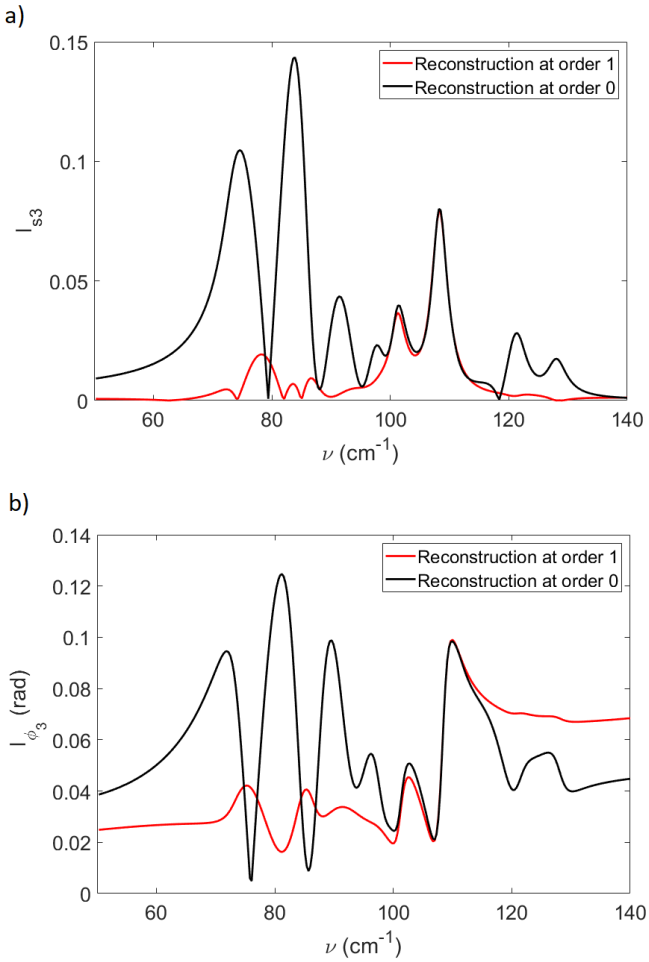

Fig. 6. Indicators I_{s_3} (a) and I_{ϕ_3} (b) as a function of the wavenumber, for the first order reconstruction (red curve), and the zero-order reconstruction (black curve) of Fig. 5.

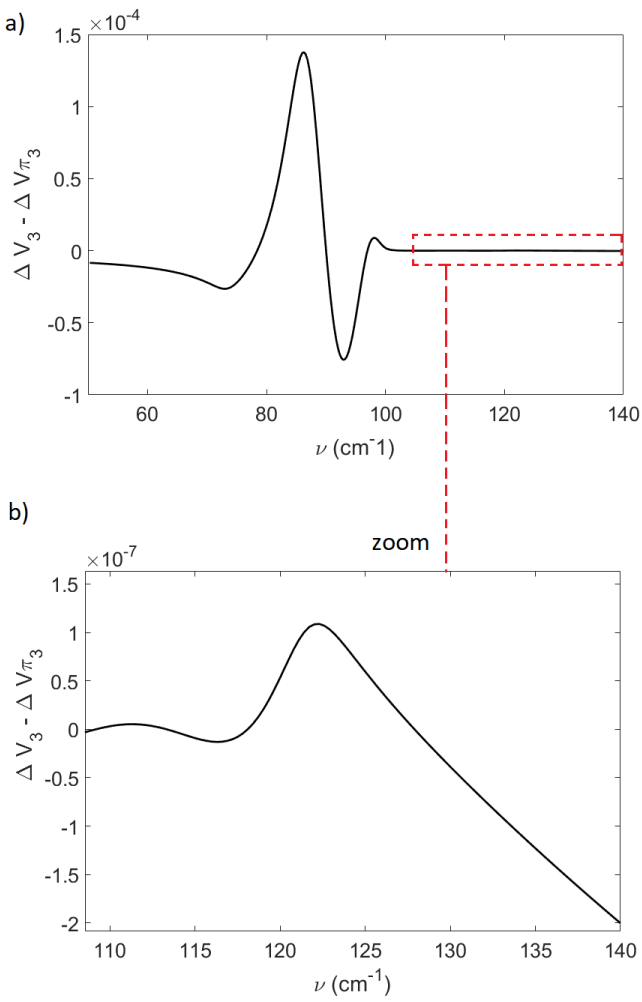

Fig. 7. a) Plot of the denominator of Eq. (36), $\Delta V_3 - (\Delta V_\pi)_3$, as a function of the wavenumber, for the first order reconstruction of Fig. 5b); b) zoom on the range of wavenumbers between 110 cm^{-1} and 140 cm^{-1}.

error, which in turn affects the efficacy of the reconstructions of ϕ_3. This method provides an accurate reconstruction of s_3 and ϕ_3, which are exploited in the experiments. By estimating these quantities, in fact, the optical properties of the sample can be extracted [5], [19]. In the next section we present a proof of principle approach to determine the dielectric permittivity of the sample; a work based on the above cited experimentally consolidated methods will be object of future investigations.

VI. Reconstruction of the Dielectric Function

The retrieval of the scattering coefficient (or, equivalently, of its harmonics) allows to reconstruct the quantity β by using the expression of α_{eff} as a function of β provided by the FD model, and the proportionality between σ and α_{eff} (see Eq. (S1) and Eqs. (S3)–(S4) in the supplementary materials). In Fig. 8 we show the reconstructed traces (red lines) for real (a) and imaginary (b) part of β by using the first order reconstruction of the harmonics σ_n with $n = 0, ..., 7$ for the case $C_{\max} = 0.13$ discussed in Sec. V, compared with the reference curves (black lines) obtained by fitting experimental data for the dielectric function of CsBr [16]. We observe a good agreement between the reconstructed and the reference curves.

In addition, a precise identification of the phonon resonances can be provided **by inspecting the plot** of the real part of the dielectric function ε_s. In fact, the transverse optical (TO) and longitudinal optical (LO) phonon resonances occur when $Re(\varepsilon_s) = 0$ and delimit the Reststrahlen region, characterized by $Re(\varepsilon_s) < 0$. From Eq. (5) we have:

$$Re(\varepsilon_s) = \frac{1 - |\beta|^2}{1 + |\beta|^2 - 2Re(\beta)} \tag{37}$$

From Eq. (37) we note that $Re(\varepsilon_s)$ depends on both real and imaginary part of β.

In Fig. 9a) the reconstructed curve (red line) for the real part of the dielectric function, obtained from the values of β in Fig. 8 by using Eq. (37), is compared with the experimental measurements (black line). We observe a good accuracy of the reconstruction, except than in proximity of the TO phonon resonance, where the maximum and minimum of the reconstructed curve exhibit a larger absolute value than the reference one **(see Fig. 9a))**. In order to explain

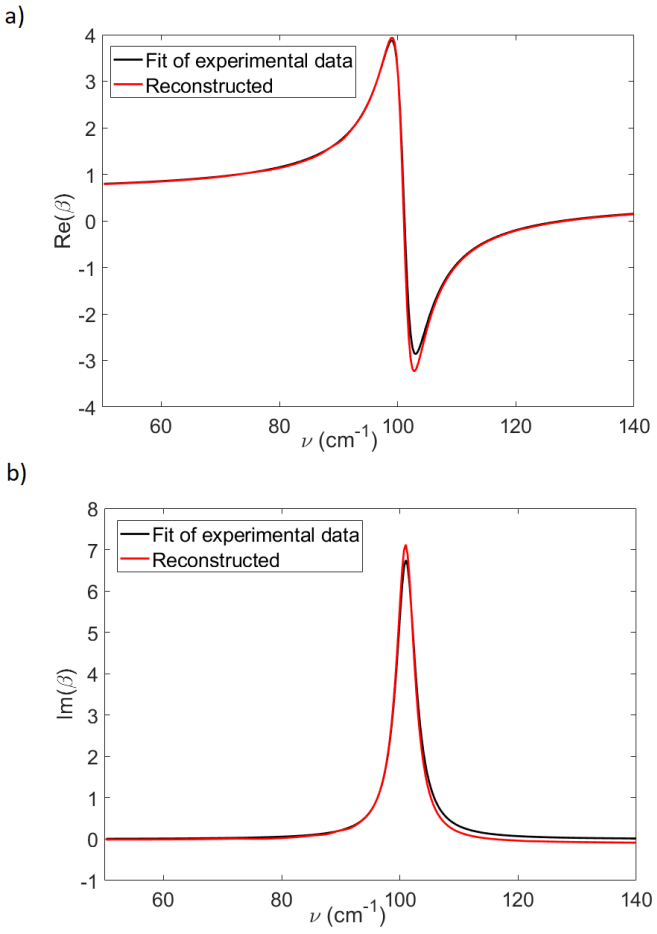

Fig. 8. Real (a) and imaginary (b) part of β as a function of the wavenumber ν. Reconstructed curves (red lines), obtained with the first order method (Eqs. (35)–(36)) for the retrieval of the harmonics σ_n, with $n = 0, ..., 7$, for $C_{\max} = 0.13$; fit of experimental data (black lines) [16].

this discrepancy, we calculated numerator and denominator of the right hand side of Eq. (37) for both reconstructed and reference curves. We noticed that both the denominators have vanishing positive values around the TO resonance, but the value of the reconstructed one is always lower for every wavenumber. Furthermore, at fixed value of ν the numerator for the reconstruction always has a higher value than that obtained from experimental data. Both these aspects (lower denominator and higher numerator) increase the value of the fraction at the right hand side of Eq. (37) and explain the discrepancy observed in Fig. 9a).

Furthermore, the fact that the denominators are always greater than zero, while the numerators vanish for slightly different values of ν explains the shift of the zero of $Re(\varepsilon_s)$ between reference and reconstruction, which can be observed in Fig. 9b): our reconstruction predicts the TO phonon at 73.19 cm^{-1}, while the reference value is 73.08 cm^{-1}. If we look at the other zero of $Re(\varepsilon_s)$, which defines the LO phonon resonance and the upper border of the Reststrahlen region, we also observe a shift of the same order of magnitude (Fig. 9c)). Therefore, even though the presence of a denominator close to zero in the formula for the retrieval of $Re(\varepsilon_s)$ affects the accuracy of the reconstruction around the TO resonance, the position of the phonons is predicted to an accurate degree, with an error of 0.1% for the TO and 0.07% for the LO phonon resonance.

VII. Conclusion

We propose a proof of principle theoretical study of a SD s-SNOM configuration exploiting a THz QCL as a laser source and detector, applied for the analysis of a sample of a CsBr, a material which presents two phonon resonances in the THz range. We developed an approximated theory based on first order Taylor expansion of the laser frequency around the free laser one valid in the weak feedback regime, for the retrieval of the scattering coefficient and its harmonics, showing that an improvement in the accuracy of the reconstruction is provided with respect to the zero-order theory only valid in the regime of very weak feedback. **We applied this method to a numerically simulated self-mixing signal in order to derive the dielectric permittivity of an hypothesized CsBr sample, and could come up with an accurate evaluation of the frequencies of the TO and LO phonon resonances characteristic of the material optical response in the THz region of the electromagnetic spectrum. Indeed, this method can be applied to any experimentally measured self-mixing SNOM signal with analogous benefit.**

Acknowledgment

The authors would like to thank to G. Scamarcio from Universita‘ degli Studi di Bari (Italy), X. Guo and K. Bertling from The University of Queensland (Australia), for interesting suggestions and fruitful discussions.

References

[1] David Richards, Anatoly Zayats, Fritz Keilmann, and Rainer Hillenbrand. Near-field microscopy by elastic light scattering from a tip. *Philosophical Transactions of the Royal Society of London. Series A: Mathematical, Physical and Engineering Sciences*, 362(1817):787–805, 2004.

[2] Nenad Ocelic, Andreas Huber, and Rainer Hillenbrand. Pseudoheterodyne detection for background-free near-field spectroscopy. *Applied Physics Letters*, 89(10):101124, 2006.

[3] S. Amarie and F. Keilmann. Broadband-infrared assessment of phonon resonance in scattering-type near-field microscopy. *Phys. Rev. B*, 83:045404, Jan 2011.

[4] Xiao Guo, Xin He, Zach Degnan, Bogdan C. Donose, Karl Bertling, Arkady Fedorov, Aleksandar D. Rakić, and Peter Jacobson. Near-field terahertz nanoscopy of coplanar microwave resonators. *Applied Physics Letters*, 119(9):091101, 2021.

[5] Xiao Guo, Karl Bertling, and Aleksandar D. Rakić. Optical constants from scattering-type scanning near-field optical microscope. *Applied Physics Letters*, 118(4):041103, 2021.

[6] A. Huber, N. Ocelic, D. Kazantsev, and R. Hillenbrand. Near-field imaging of mid-infrared surface phonon polariton propagation. *Applied Physics Letters*, 87(8):081103, 2005.

[7] Hou-Tong Chen, Roland Kersting, and Gyu Cheon Cho. Terahertz imaging with nanometer resolution. *Applied Physics Letters*, 83(15):3009–3011, 2003.

[8] Aurele Joseph Louis Adam. Review of near-field terahertz measurement methods and their applications. *Journal of Infrared, Millimeter, and Terahertz Waves*, 32(8):976, Jul 2011.

[9] Maria C. Giordano, Stefan Mastel, Clemens Liewald, Lorenzo L. Columbo, Massimo Brambilla, Leonardo Viti, Antonio Politano, Kai Zhang, Lianhe Li, A. Giles Davies, Edmund H. Linfield, Rainer Hillenbrand, Fritz Keilmann, Gaetano Scamarcio, and Miriam S. Vitiello. Phase-resolved terahertz self-detection near-field microscopy. *Opt. Express*, 26(14):18423–18435, Jul 2018.

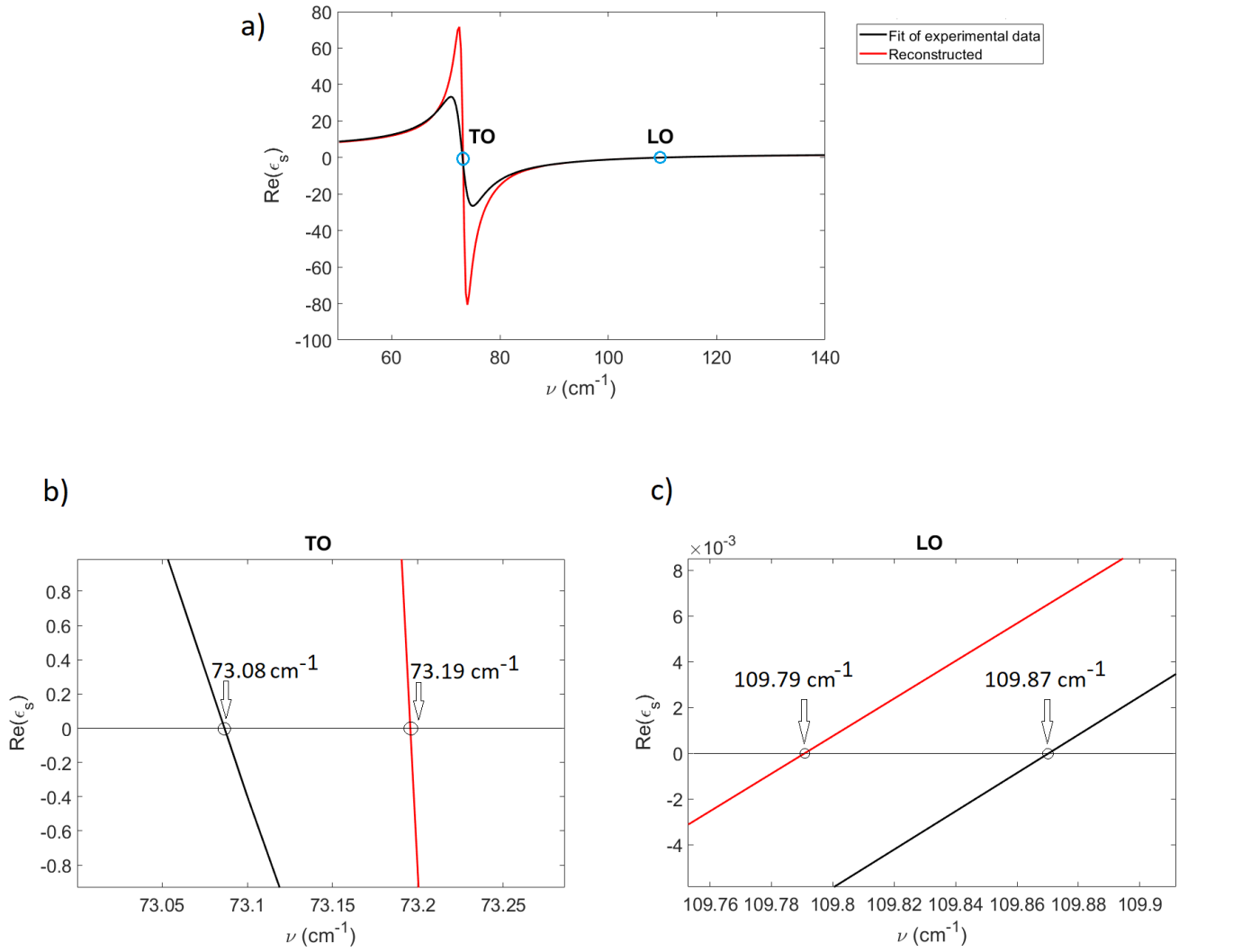

Fig. 9. a) Reconstructed curve (red line) and fitted experimental data [16] (black curve) for the real part of the dielectric function ε_s of CsBr; zoom around the TO (b) and LO (c) phonon resonances.

[10] Eva A. A. Pogna, Carlo Silvestri, Lorenzo L. Columbo, Massimo Brambilla, Gaetano Scamarcio, and Miriam S. Vitiello. Terahertz near-field nanoscopy based on detectorless laser feedback interferometry under different feedback regimes. *APL Photonics*, 6(6):061302, 2021.

[11] Eva Arianna Aurelia Pogna, Leonardo Viti, Antonio Politano, Massimo Brambilla, Gaetano Scamarcio, and Miriam Serena Vitiello. Mapping propagation of collective modes in Bi2Se3 and Bi2Te2.2Se0.8 topological insulators by near-field terahertz nanoscopy. *Nature Communications*, 12(1):6672, Nov 2021.

[12] Valentino Pistore, Eva Arianna Aurelia Pogna, Leonardo Viti, Lianhe Li, A. Giles Davies, Edmund H. Linfield, and Miriam Serena Vitiello. Self-induced phase locking of terahertz frequency combs in a phase-sensitive hyperspectral near-field nanoscope. *Advanced Science*, 9(28):2200410, 2022.

[13] R. Lang and K. Kobayashi. External optical feedback effects on semiconductor injection laser properties. *IEEE Journal of Quantum Electronics*, 16(3):347–355, 1980.

[14] Thomas Taimre, Milan Nikolić, Karl Bertling, Yah Leng Lim, Thierry Bosch, and Aleksandar D. Rakić. Laser feedback interferometry: a tutorial on the self-mixing effect for coherent sensing. *Adv. Opt. Photon.*, 7(3):570–631, Sep 2015.

[15] Deborah M. Kane and K. Alan Shore, editors. *Unlocking Dynamical Diversity: Optical Feedback Effects on Semiconductor Lasers*. John Wiley & Sons, United States, December 2005.

[16] Edward D. Palik. *Handbook of optical constants of solids*. Orlando, Academic Press, 1985.

[17] Russell Kliese, Thomas Taimre, A. Ashrif A. Bakar, Yah Leng Lim, Karl Bertling, Milan Nikolić, Julien Perchoux, Thierry Bosch, and Aleksandar D. Rakić. Solving self-mixing equations for arbitrary feedback levels: a concise algorithm. *Appl. Opt.*, 53(17):3723–3736, Jun 2014.

[18] We do not calculate a relative error also for ϕ, because it would be possible to reduce it arbitrarily by shifting all the values of ϕ_{calc} (which would appear in the denominator of the relative error expression) by a generic multiple of 2π. Then, this analysis would result unreliable.

[19] Alexander A. Govyadinov, Iban Amenabar, Florian Huth, P. Scott Carney, and Rainer Hillenbrand. Quantitative measurement of local infrared absorption and dielectric function with tip-enhanced near-field microscopy. *The Journal of Physical Chemistry Letters*, 4(9):1526–1531, 2013. PMID: 26282309.

Carlo Silvestri obtained his Master's degree in Physics at University of Bari (Italy) in 2018, and his PhD in Electronics Engineering at Polytechnic University of Turin (Italy) in 2022. He joined the University of Queensland in 2022, where he is currently a Postdoctoral Research Fellow at the School of

Information Technology and Electrical Engineering. His research interests are laser dynamics, photonics, and optoelectronic devices, with applications for imaging, spectroscopy, and communication systems. His research is currently focused on the study of the of the dynamics of terahertz quantum cascade lasers, with a particular interest in the generation of optical frequency combs, and in the study of near-field optical microscopy based on this laser source.

Lorenzo Luigi Columbo received the M.Sc. degree in physics from the Universitá deli Studi di Bari, Bari, Italy, in 2002 and the Ph.D. degree in physics and astrophysics from the Dipartimento di Scienza e Alta Tecnologia, Universitá degli Studi dell'Insubria, Como, Italy, in 2007. He worked as post-doc at Institut Nonlinéaire de Nice, Valbonne, France, Dipartimento di Fisica of the Universitá degli Studi di Bari, Bari, Italy and at the Dipartimento di Scienza e Alta Tecnologia, Universitá degli Studi dell'Insubria, Como, Italy. In April 2016, he joined the Dipartimento di Electronica e Telecomunicazioni of the Politecnico di Torino, Torino, Italy where he became associate professor in November 2022. His recent theoretical research activity focuses on optical frequency combs generation in single section Quantum Dot lasers and Quantum Cascade Lasers and on the modeling of hybrid laser dynamics in silicon photonics platforms. His main fields of interest are quantum electronics, optoelectronics, and nonlinear optics.

Massimo Brambilla was born in Milan, Italy in 1961. He received the Laurea in Physics at the University of Milan (IT) in 1988 and the Dokt.Phil. at the University of Zuerich (CH) in 1992. He is an associate professor in laser and optical physics at the Politecnico di Bari, active in the study of laser spatiotemporal dynamics, optical solitons, optical comb formation, etc. He authored about 180 publications in journals, volumes and proceedings.